NASA TECHNICAL NOTE

NASA TN D-6593

FIELD EVAPORATION ION SOURCE WITH POSSIBLE APPLICATION TO ELECTROSTATIC PROPULSION

by Victor G. Weizer

Lewis Research Center
Cleveland, Ohio 44135

NATIONAL AERONAUTICS AND SPACE ADMINISTRATION • WASHINGTON, D. C. • DECEMBER 1971

1. Report No.	2. Government Accession No.	3. Recipient's Catalog No.
NASA TN D-6593		

4. Title and Subtitle	5. Report Date
FIELD EVAPORATION ION SOURCE WITH POSSIBLE APPLICATION TO ELECTROSTATIC PROPULSION	December 1971
	6. Performing Organization Code

7. Author(s)	8. Performing Organization Report No.
Victor G. Weizer	E-6540
	10. Work Unit No.

9. Performing Organization Name and Address	114-03
Lewis Research Center	11. Contract or Grant No.
National Aeronautics and Space Administration	
Cleveland, Ohio 44135	13. Type of Report and Period Covered

12. Sponsoring Agency Name and Address	Technical Note
National Aeronautics and Space Administration	14. Sponsoring Agency Code
Washington, D.C. 20546	

15. Supplementary Notes

16. Abstract

Field evaporation of solid metal electrodes has been proposed as an ion source for an electrostatic propulsion device. The chief advantage over existing ion sources is the prospect of 100 percent fuel utilization efficiency. This advantage arises as a result of the elimination of the need for a gaseous precursor state for propellant ionization. The attainment of required high surface field strengths is achieved through field-induced extrusion of the electrode geometry at elevated temperatures. Contributions of both surface and bulk transport mechanisms are taken into account.

17. Key Words (Suggested by Author(s))	18. Distribution Statement
Field evaporation	Unclassified – unlimited
Electrostatic propulsion	

19. Security Classif. (of this report)	20. Security Classif. (of this page)	21. No. of Pages	22. Price*
Unclassified	Unclassified	21	$3.00

FIELD EVAPORATION ION SOURCE WITH POSSIBLE APPLICATION

TO ELECTROSTATIC PROPULSION

by Victor G. Weizer

Lewis Research Center

SUMMARY

Field evaporation of solid metal electrodes has been proposed as an ion source for an electrostatic propulsion device. The chief advantage over existing ion sources is the prospect of 100 percent fuel utilization efficiency. This advantage arises as a result of the elimination of the need for a gaseous precursor state for propellant ionization. The attainment of required high surface field strengths is achieved through field-induced extrusion of the electrode geometry at elevated temperatures. Contributions of both surface and bulk transport mechanisms are taken into account.

INTRODUCTION

The purpose of a propulsion device is to apply a force to a payload for a given period of time. The net result of this force acting over a period of time t is known as the impulse J. It can be seen from the relation

$$J = \int_0^t F \, dt = mv_2 - mv_1 = m\Delta v$$

where F is the applied force, m is the vehicle mass, and v_1 and v_2 are the initial and final vehicle velocities, respectively, that the impulse is the change in vehicle momentum due to the applied force. In order to apply an impulse J to the vehicle, a rocket engine must apply an equal and opposite impulse to the ejected fuel. The means of producing the required impulse in the ejected fuel depends upon the relative abundance or shortage of energy and propellant. If it happens that there is a severe limit on the amount of propellant available, the logical approach is to use an engine that produces

very large exhaust velocities. This would result in a high accelerating force F, defined by

$$F = \dot{m}v$$

where v is the exhaust velocity, combined with a low rate of propellant mass flow $\dot{m}$. In other words, using high exhaust velocities reduces the required mass flow rate for a given accelerating force and thus conserves propellant.

If we consider, however, the power required to produce a given exhaust velocity, we see that it is proportional to the square of the exhaust velocity. Thus, the power required to produce an exhaust velocity v is

$$P = \frac{1}{2}\dot{m}v^2$$

If we now take the ratio of P to F, we see that

$$\frac{P}{F} = \frac{v}{2}$$

of that the power to produce a unit of thrust goes up linearly with the exhaust velocity. Therefore, we must come to some compromise between the need to conserve propellant on one hand and the availability of power on the other.

One measure of the exhaust velocity is the specific impulse I_s, defined as

$$I_s = \frac{v}{g} \quad \text{(sec)}$$

where g is the gravitational acceleration. It seems that a value of about $5{\times}10^3$ seconds (ref. 1) is the maximum that the present power supply technology makes feasible. For missions where power might not be a consideration, however, the higher the specific impulse, the better.

The ion engine is a high-specific-impulse propulsion device. It consists of a means of ionizing a propellant and a means of accelerating these ions to high velocities in an electrostatic field. The two types of engines that have received most attention are the mercury electron bombardment (MEB) engine and the cesium contact ionization (CCI) engine. Of the two, only the former has been developed to a state where it can be tested in space.

Inherent in these two types of engines are fuel utilization inefficiencies due to the fact that the propellant material must be in the gaseous state either before or during

ionization. Thus problems of containing the gas until it is ionized and accelerated arise (refs. 2 and 3). The problem is particularly severe in the case of the low-thrust ($>22.5 \times 10^{-4}$ N; 0.5 mlb) MEB engine, where propellant losses of 40 to 50 percent are seen (ref. 4). Containment of gaseous propellant was also the reason why field ionization was rejected as a potential ion source (ref. 5).

There is one method of producing ions, however, which does not involve the gaseous phase of the propellant, that is, field evaporation. Field evaporation is the ionization and removal of surface atoms from a solid material under the influence of very high electrostatic fields (1×10^{10} to 6×10^{10} V/m; 1 to 6 V/Å). The fact that 100 percent fuel utilization is attendant to this method of ionization suggests further investigation of possible use in an electrostatic ion engine.

After a brief description of the field evaporation process itself, this report investigates the mechanisms that theoretically could limit the current density (and thus the thrust) obtainable from such an ion source.

FIELD EVAPORATION

The process of field evaporation was discovered during the development of the field-ion microscope several years ago (ref. 6). It is, in fact, an indispensible tool in field-ion microscopy in that it is used to remove surface roughness from a field-ion specimen and produce the perfectly clean, smooth surfaces that are needed in order to study surface phenomena on an atomic scale. The process is also used to strip or peel away the surface layers in order to investigate the interior of the specimen. Evaporation rates range from a few atoms per second to many billions of atoms per millisecond.

The phenomenon of field evaporation is quite complex and not fully understood at the present time. However, the general nature of the process is known and it is possible to predict the fields necessary for field evaporation of most important metals within about 10 or 15 percent. A description of the mechanisms involved in field evaporation is aided by referring to the potential diagram in figure 1.

Basically, field evaporation is the thermal activation of a surface atom over a small, residual, field-dependent energy barrier. With no field applied, the energy required to remove a surface atom in a singly charged state Q_0 consists of the evaporation energy to remove an atom to an infinite distance from the lattice Λ, and the ionization energy to ionize the atom I. If the removed electron is then returned to the lattice, an energy equal to the work function φ is regained by the system. Thus, in the absence of a field

$$Q_0 = \Lambda + I - \varphi$$

As the ion is brought close to the surface, its potential energy can be described by the image potential

$$V_I = - \frac{n^2 e^2}{4x}$$

where x is the distance from the surface and ne is the charge on the ion.

The application of a field F to the surface results in deformation of the ionic potential curve such as shown in figure 1(b). As a result of the field, the energy barrier Q can be seen to be much smaller than Q_0. The barrier reduction is due to the combined effects of the image potential V_I and the potential due to the applied field V_F, where

$$V_F = - neFx$$

The result is a field-dependent activation barrier given by

$$Q = Q_0 - \frac{n^2 e^2}{4x} - neFx$$

To a first approximation, the evaporation field F_e can be defined as that field for which Q vanishes:

$$F_e = \frac{\Lambda + I - \varphi - \dfrac{n^2 e^2}{4r_0}}{ner_0}$$

where r_0 is the atomic radius of the atom to be evaporated. Calculated values of F_e with $n = 1, 2$ (ref. 7) are given in table I for a number of metals and semiconductors. It can be seen that, in many cases, doubly charged ions are predicted to evaporate at lower fields than the singly charged species. Some experimentally derived evaporation fields are given for comparison (ref. 7).

It can be seen from table I that the fields required to produce field evaporation are very high. Fields of this magnitude, $>10^{10}$ volts per meter (1V/Å), can only be attained at reasonable voltages (V $<$ 40 kV) by going to a special electrode geometry.

If a wire-shaped electrode is oriented in such a way that its axis is perpendicular to a large planar electrode, moderate voltages applied between the two can result in extremely high fields at the end of the wire electrode because of the very small radius of curvature there. This geometrical arrangement seems to be the only one that will

4

satisfy the field strength requirements of the proposed field evaporation ion source. Thus, the following discussion is concerned only with these wire-shaped electrodes. This geometrical restriction is, however, compatable with the need for continuous feed of propellant, as the wire can be fed into the evaporation chamber from storage spools.

Because the weight of an ion engine increases with size, it is desirable to keep the engine dimensions as small as possible while still producing significant thrust (ref. 8). Further, because the thrust is directly proportional to the ion current produced, the engine should be capable of operating at reasonably high current densities. At first glance, there appear to be two possible current-density limiting mechanisms: (1) space-charge limitations, and (2) field-evaporation-rate limitations. Let us consider each in turn.

SPACE-CHARGE LIMITATIONS

In order to obtain an estimate of the maximum current density that can be drawn before space-charge effects come into play, one must solve Poisson's equation for the electrode geometry under consideration while imposing suitable boundary conditions. For a plane diode engine such as the CCI engine the problem is straightforward. The boundary conditions are such that ions can be drawn from the source until the space charge shields the source to such an extent that the field at the emitting surface vanishes.

The situation is more complex, however, where high surface fields are required to create the ions, such as in the case of field evaporation. In this case the current ceases as the field is lowered below a relatively high value.

Investigation of the effect of space charge on field-electron emission from needle-shaped emitters (ref. 9) has shown, however, that current densities of 10^8 amperes per square centimeter can be obtained experimentally at surface field strengths of about 10^{10} volts per meter (1 V/Å).

At this point it should be noted that for the remainder of the report the term field strength refers to the local field strength at the surface of the electrode being discussed.

Since the limiting current density is proportional to the inverse square root of the ion mass, these electron emission results can be extended to the present case of field evaporation of heavy ions by introducing a correction factor $(m_e/m_i)^{1/2}$, where m_e and m_i are the masses of an electron and a field-evaporated ion, respectively. The resulting space-charge-limited current density as a function of ion mass is plotted in figure 2. For tungsten ions, $m_i = 184$, the limit seems to be of the order of 10^5 amperes per square centimeter.

It should be noted that the actual ion source area is, to a first approximation, the cross-sectional area of the emitter wire. In order to compare these results with those from other ion sources, an effective current density can be calculated that takes into consideration the actual spatial arrangement of the field-evaporation source electrodes. If

5

we assume the engine area occupied by one emitting wire and its accelerating electrode A' to be about 0. 25 square centimeter (fig. 3), then we can calculate an effective current density J from the relation

$$J = j \frac{A}{A'}$$

where A is the cross-sectional area of the emitting wire, and j is the actual space-charge-limited current density. A plot of J as a function of ion mass is given in figure 3, where an emitter radius of 10^{-4} centimeter has been assumed. The resulting values ($\sim$20 mA/cm^2 for tungsten) are comparable with those obtained with existing engines which produce current densities between 0. 1 and 10 milliamperes per square centimeter (refs. 2 and 10).

Because tungsten is the most convenient metal for use in both field-ion and field-emission microscopy, its properties, or at least the ones of interest here, have been studied more intensively than those of any other material. Because of the availability of data in the literature, the remainder of this report is concerned with calculations performed with tungsten as the propellant material.

FIELD-EVAPORATION LIMITATIONS

Let us now consider the second possible current limiting mechanism, the field-evaporation process itself. Theoretical analysis is difficult here, but reported values of evaporation rates can give an indication of what order of magnitude one can expect.

Investigations performed with the atom-probe time-of-flight mass spectrometer (ref. 7) show that evaporation rates of 3×10^9 atom layers per second can easily be obtained. Furthermore, these dissolution rates were observed for tungsten, which, according to the data presented in table I, is one of the most difficult materials to field evaporate. For a wire radius of 10^{-5} centimeter, which was used in this experiment (ref. 7), a calculated effective current density greater than 1 milliampere per square centimeter is indicated. Therefore, no serious limitation of current density is expected to arise from the field-evaporation mechanism itself.

GEOMETRICAL CONSIDERATIONS

The surface fields necessary to field evaporate a material like tungsten are quite high, that is approximately 5×10^{10} volts per meter (5 V/Å). In order to obtain surface fields of this magnitude, one must manipulate the geometry of the electrodes in such a

way as to obtain a high charge density on the surface. This can be done by reducing the size of one of a pair of electrodes to very small dimensions. In the case at hand, where the surface to be considered is the end of a small wire, the surface field is inversely proportional to the radius of the wire. A plot of the field strength, in volts per meter ($V/\mathring{A}$), on the end of a small wire electrode is given as a function of wire radius for several values of applied voltage in figure 4. To the author's knowledge the smallest commercially available wire has a radius in the region of 10^{-4} centimeter. According to figure 4, this value would be too large to permit field evaporation of the wire atoms at reasonable voltages.

Extremely high voltages could be applied, but they would result in very high ion exhaust velocities and thus high specific impulse unless the ions were subsequently decelerated before they left the engine. Furthermore, high voltages are hard to handle in a practical sense, because they require good insulation and greater electrode separations, both of which tend to increase the size and weight of the propulsion system. It seems that some means of making the geometry of the wire more suitable for low-voltage operation is called for.

Surface Transport

A solution to the problem is suggested in some brilliant work in the literature by Dyke, Charbonnier, Strayer, Floyd, Barbour, and Trolan (ref. 11) and Bettler and Charbonnier (ref. 12). It is well known that, at sufficiently high temperatures, small crystals of most materials tend to alter their geometry, by surface self-diffusion, in such a way as to reduce the total crystal energy. Such a mechanism, when applied to a needle-shaped crystal such as shown in figure 5, tends to produce balling at the point. In this case atoms near the apex of the point diffuse toward the shank when the temperature is raised to permit surface diffusion. The effect of this migration is to lower the total crystal energy. The rate of diffusion toward the shank as a function of the temperature T can be given in terms of the surface tension γ and the tip radius r by the expression

$$\left.\frac{dz}{dt}\right)_0 = -\frac{\gamma \Omega_0^2 D_0 \exp{-\frac{Q}{kT}} \, (1.25)}{A_0 kT r^3} \tag{1}$$

where $dz/dt)_0$ is the rate of change of the length of the needle, Ω_0 and A_0 are the atomic volume and surface area, respectively, D_0 is the diffusivity constant, and Q is the activation energy for surface diffusion.

Now let us consider the case where an electric field is applied to the needle. The field strength will vary along the surface in such a way that the field is a maximum at the apex and falls off with distance from the apex. The degree of this field inhomogeneity is plotted in figure 6 (ref. 13) The effect of the field on the surface is to cause polarization of the surface atoms. These polarized atoms, if they are thermally activated so as to be able to migrate over the surface, are drawn to the regions of the surface where the field strength is the greatest. Thus, if the atoms are sufficiently thermally activated, the effect of an applied field on a needle-shaped electrode is to produce migration from the lower field regions on the shank to the high field regions around the apex. This field-induced surface diffusion would oppose the previously discussed thermal blunting diffusion. It has been shown, in fact, that these two mechanisms can be made to balance one another when the conditions of field and temperature are adjusted to the proper values.

The rate of change of wire length under the influence of a surface field F_0 has been shown to be (ref. 11)

$$\left(\frac{dz}{dt}\right)_{F_0} = \left(1 - \frac{rF_0^2}{16C_0\pi\gamma}\right)\left(\frac{dz}{dt}\right)_0 \tag{2}$$

where $(dz/dt)_0$ is the thermal blunting rate given by equation (1), and C_0 is a geometrical constant (≈ 0.5). It is apparent that the condition for zero net migration is that the first term on the right vanish. Thus, the field strength needed to stop thermal blunting F_{01}, regardless of the wire temperature, is

$$F_{01} = \left(\frac{8\pi\gamma}{r}\right)^{1/2} \tag{3}$$

Because of some second-order effects that come into play at fields slightly above F_{01}, however, it has been determined that equation (3) does not hold precisely, and that, in fact, a field F_{02} must be applied to prevent thermal blunting, where (ref. 11)

$$F_{02} = \sqrt{2}\, F_{01} \tag{4}$$

At field strengths above F_{02}, then, the net migration of the surface atoms is toward the apex of the tip, and below F_{02} the direction of migration is toward the shank.

The question that now arises is whether reasonable values of applied voltage can produce sufficiently high fields at the surface to promote a net migration toward the apex.

8

The critical field F_{02} is plotted in figure 4 as a function of tip radius. For any value of tip radius, fields above F_{02} will induce the desired tip extrusion.

Since the smallest commercially available wire sizes range between 10^{-3} and 10^{-4} centimeter in radius, it can be seen that voltages of approximately 20 kilovolts or greater will be sufficient to produce the field extrusion effect.

We now have a method of changing the geometry of the propellant wire at will. Specifically, if we apply a sufficiently high field $(>F_{02})$ to the thermally activated wire, we should be able to extrude the wire to very small dimensions near the apex. The high fields present near this region of very small radius of curvature should then be sufficient to permit rapid field evaporation.

A closer look at the field extrusion process (ref. 12), however, shows that it is not a simple extrusion of the end of the wire. It seems that the activation barrier to the nucleation of new planes on top of existing planes is quite high. For this reason the extrusion takes place in such a way as to extend or build up the major low-index planes. (For tungsten these are the (110), the (211), and the (001).) The resulting geometry consists of large flat facets, meeting at very sharp angles such as shown in figure 8 of reference 7. The regions of intersection of the facets are regions of very high field strength. The resulting geometry closely approximates a pyramidal protrusion from the surface of height $h \approx 0.1\,r$, where r is the wire radius. The field strength at the apex of the protrusion can be calculated from Drechsler's relation (ref. 14)

$$F_P = F_0 \left(\frac{h}{R}\right)^{1/2}$$

where F_0 is the surface field strength in the absence of a protrusion, and R is the radius of a surface atom. For a wire radius of 10^{-4} centimeter, therefore, an apex field strength of about $17\,F_0$ is expected. This corresponds to fields that are twice as great as those needed to promote field evaporation.

Thus, we can conclude that, with moderate voltages (10 to 40 kV) applied to a wire electrode, field-induced extrusion will occur with the result that the geometry of the tip is changed so as to make possible continuous field evaporation of the wire atoms.

The next question concerns the limitation of the current density by the field-induced surface migration rate. We can get an idea of the magnitude of the atomic flow rate by considering the following expression for the time required to obtain a characteristic degree of facet buildup at the end of the tungsten emitter t_M (ref. 11)

$$t_M = 2.18 \times 10^{18}\ T \exp \frac{Q}{kT}\ \frac{r^3}{F^2 - F_{02}^2} \tag{5}$$

where F is the surface field strength.

This characteristic buildup requires the transport of a volume of material v (estimated in ref. 11 to be $\approx 0.02\, r^3$) from the low field to the high field regions.

The volume flow rate can then be written

$$\frac{dV}{dt} = \frac{v}{t_M} = \frac{0.02\, r^3}{t_M}$$

Then, if $\dot{N}$ is the atomic flow rate in atoms per second,

$$\dot{N} = \frac{v}{\Omega t_M} = 5.76 \times 10^{12} \frac{F^2 - F_{02}^2}{T} \exp{-\frac{Q}{kT}} \quad \frac{\text{atoms}}{\text{sec}}$$

If it is assumed that all the migrating atoms are eventually ionized in the field-evaporation process, an expression for the expected ion current can be obtained:

$$I = 0.96 \times 10^{-13}\, q\, \frac{F^2 - F_{02}^2}{T} \exp{-\frac{Q}{kT}} \quad \text{(ma)} \tag{6}$$

where q is the ionic charge state.

In figure 7 the expected ion current from a 10^{-4}-centimeter radius tungsten emitter wire is plotted as a function of emitter temperature. It can be seen that currents from 10^{-5} to 10^{-4} milliampere are predicted for temperatures in the neighborhood of $0.9\, T_m$, where T_m is the bulk melting temperature.

The use of equation (6) at high temperatures, however, does not seem to be fully justified in that, as the temperature approaches $\sim 0.75\, T_m$, surface melting occurs wherein the surface lattice structure upon which equation (6) is based breaks down (ref. 15). This is equivalent to a reduction in the activation energy for surface diffusion.

We would expect, therefore, to observe a deviation from linearity in a plot of log D against $1/T$ as the temperature approaches that required to cause surface melting and the attendant destruction of crystalline order on the surface. This deviation is indeed observed for the surface self-diffusion of tungsten at temperatures as low as $0.69\, T_m$ (ref. 16). When this deviation is extrapolated to $0.93\, T_m$, an estimated diffusion enhancement factor of about 10^4 is indicated. At $0.93\, T_m$, then, a current of 0.3 milliampere is estimated for tungsten. Thus, for an emitting area of 0.25 square centimeter, an effective current density of approximately 1 milliampere per square centimeter is obtained. This is essentially the same as the previously considered field-evaporation-

limited current density. It is difficult, therefore, to judge which of the two is the rate-limiting process at these high temperatures.

Because of the fact that the current densities obtained with the MEB engine are also of the order of 1 milliampere per square centimeter, the expected thrust levels from a field-evaporation engine should be comparable with those from an MEB engine of similar emitting area.

Bulk Transport

Up to this point we have been considering the deformation of emitter geometry by means of surface transport, and the results of the calculations show that the rates involved should be sufficient to obtain current-density levels comparable with those of existing electrostatic engine ion sources. These current densities are obtained, however, at the expense of going to high electrode temperatures and thus introduce thermal inefficiencies. It would be desirable if this requirement could be at least partially alleviated.

Fortunately, field-induced surface migration is not the only phenomenon that can be called upon to alter the geometry of the emitter wire. Bulk transport by thermally activated slip in the high field regions of the surface has been reported to produce protrusions from the surface which result in greatly enhanced field-evaporation effects (ref. 17). However, since these effects have been considered nuisances or hinderances to the use of the field-ion microscope, little work has been done to identify the factors influencing this type of behavior.

By scouring the literature, however, an indication of the relation between field strengths and temperature necessary to promote bulk slip can be obtained. Table II lists the fields and temperatures at which field-induced slip has been experimentally observed. With the exception of, perhaps, points 1 and 5 (temperatures of 1000 and 1800 K), these data do not necessarily represent the minimum fields required for slip to occur, but they do serve to give a conservative lower limit to the region of plastic flow.

The magnitude of the stresses acting on the surface of the tip can be shown to be proportional to the square of the surface field strength. Thus,

$$\sigma = AF_0^2$$

where σ is the field-induced stress, and A is the constant of proportionality. At a given temperature, therefore, the lowest field strength at which slip occurs can be used to calculate the yield strength of the material being observed, if A is known.

Because of uncertainties in the value of A, in figure 8, the square of the surface field, rather than σ, is plotted as a function of reciprocal temperature for the data of table II. The form of this curve is quite similar to macroscopic measurements of the

yield strength taken on polycrystalline samples (ref. 18). At points below the curve one would expect only surface transport processes to be active, whereas above the curve both surface transport and bulk slip will occur.

In order to extrapolate the table II data to higher temperatures (and lower fields), it is more convenient to plot the data logarithmically as in figure 9. It can be seen that for attainable values of the field strength ($F < 0.7 \times 10^{10}$ V/m; 0.7 V/Å) plastic flow of the emitter wire is expected to occur at temperatures above about 0.38 T_m.

At this point the question that presents itself is whether the wire will fail plastically somewhere along its shank at temperatures or fields below those at which sufficient ion current can be drawn.

Again we can, by making use of published data, set a conservative upper limit to the usable range of field and temperature. Let us start by making the reasonable assumption that the field-induced tensile stress acting in the shank of the wire is less by some factor B, let us say, than the stress acting on the regions of high curvature at the end of the wire. Thus, if we take from the literature the values for the highest field-temperature combination that are consistent with stable operation (no shank failure) and assume these to be a conservative lower limit for the conditions for shank failure, we can find an effective ratio of shank yield stress to surface yield stress. Thus,

$$\left(\frac{F_S}{F_E}\right)^2 = B \tag{7}$$

where F_S is the surface field required to produce slip in the shank, and F_E is the field required to produce slip in the apex region, both measured at the same temperature.

Drechsler (ref. 14) has published data showing stable operation at 2400 K at a field strength of 0.7×10^{10} volts per meter (0.7 V/Å). According to figure 9 the field strength required to initiate plastic flow in the apex region at the same temperature is about 0.375×10^{10} volts per meter (0.375 V/Å). Therefore, from equation (7) we find that

$$B = \left(\frac{0.7}{0.375}\right)^2 = 3.5$$

This means that the field-induced stresses present at the sharply curved regions on the end of the wire are at least $3\frac{1}{2}$ times greater than those acting in the shank of the wire for a given applied voltage. Shank failure at any temperature, then, would require fields

that are at least 1.87 (i. e., $\sqrt{3.5}$) times greater than those which promote slip at the end of the wire.

The resulting lower limit to shank failure is given by the dashed curve in figure 9. It can be seen that shank failure should not be a problem for the conditions under consideration, that is, $F < 0.5 \times 10^{10}$ volts per meter; (0.5 V/Å), $T < 3400$ K.

Estimates of the increase in field evaporation rates which would result from the apex slip phenomenon are difficult to make. It has been reported (ref. 17) that, once the field-temperature yield point has been exceeded, a minimum evaporation rate of about 2 atom layers per second obtains. An estimate of the evaporation rate at higher temperatures or fields, however, cannot be made with any confidence. While it is certain that these slip mechanisms will increase the rate of ion production, one can only speculate as to how great a reduction of the required electrode temperatures can be expected. Only further work on the measurement of evaporation rates at high temperatures will yield the answer.

As was mentioned previously, the choice of tungsten as the propellant material in this study was made because of the availability of tungsten data in the literature. Tungsten does, however, have several properties that are not consistent with being the best suited material for an ion source. First, it has a very high evaporation field (table I). A reduction in the required applied voltage by a factor of 2 or 3 is seen to be possible by the selection of a more easily ionizable material. Second, because tungsten possesses the highest melting temperature of all the elements, the activation of surface and bulk transport mechanisms requires temperatures that are significantly higher than those that would be needed if a less refractory material were used.

A systematic search for the optimum propellant material, therefore, is certainly in order.

SUMMARY OF RESULTS

Field evaporation of wire-shaped tungsten electrodes has been considered as a source of ions for an electrostatic propulsion engine. Limitations on the attainable current-density levels due to both space-charge effects and inherent limitations of the evaporation process itself were investigated. The resulting calculations show that current-density levels comparable to those of existing ion engines can be produced.

Problems relating to electrode geometry arise when an attempt is made to obtain sufficiently high field strengths on the surface of the electrode without applying unreasonably high voltages. These problems were solved by invoking thermally activated and field-directed surface and bulk transport processes which alter the electrode geometry in such a way as to provide sufficient surface fields with reasonable applied voltages.

Invoking only the surface transport mechanism showed that current-density levels comparable to those of existing ion engines can be obtained. If bulk transport is also considered, a reduction in operating temperatures, that is, greater thermal efficiency, can be effected.

It should be noted that this report concerned solely the ability of a field evaporation ion source to produce a sufficient current density so as to be comparable with existing engines. Hence, problems that arise when dealing with a specific ion engine such as total power dissipation, beam focussing, propellant feed, electrode sputtering, etc. were not considered.

A problem also arises when one considers the high exhaust velocities created by the field-evaporation source. With the aid of an acceleration-deceleration system, however, it should be possible to reduce the resultant high specific impulse to an acceptable value.

It can be concluded from the preceding discussion that the application of field evaporation to ion propulsion is a feasible concept and should be investigated more fully. The main advantage offered by the field-evaporation engine over existing engines is the prospect of 100 percent fuel utilization efficiency.

Lewis Research Center,
    National Aeronautics and Space Administration,
        Cleveland, Ohio, September 23, 1971,
            114-03.

REFERENCES

1. Zola, Charles L.: Interplanetary Probe Missions with Solar-Electric Propulsion Systems. NASA TN D-5293, 1969.

2. Pawlik, Eugene V.; and Nakanishi, Shigeo: Experimental Evaluation of Size Effects on Steady-State Control Properties of the Electron-Bombardment Ion Thrustor. NASA TN D-2470, 1964.

3. Kaufman, Harold R.: Performance Correlation for Electron-Bombardment Ion Sources. NASA TN D-3041, 1965.

4. Kerslake, William R.; Wasserbauer, Joseph F.; and Margosian, Paul M.: A Mercury Electron-Bombardment Ion Thrustor Suitable for Spacecraft Station Keeping and Attitude Control. Paper 66-247, AIAA, Mar. 1966.

5. Stankiewicz, Norbert: Feasibility of Applying Field-Ion Emission to Electrostatic Rocket Engines. NASA TN D-1563, 1963.

6. Müller, Erwin W.: Field Ionization and Field Ion Microscopy. Advances in Electronics and Electron Physics. Vol. 13. L. Morton, ed.; Academic Press, 1960, pp. 83-179.

7. Müller, Erwin W.: Field Ion Microscopy. American Elsevier Publ. Co., 1969.

8. Sutton, George P.: Rocket Propulsion Elements. Third ed., John Wiley & Sons, Inc., 1963.

9. Barbour, J. P.; Dolan, W. W.; Trolan, J. K.; Martin, E. E.; and Dyke, W. P.: Space-Charge Effects in Field Emission. Phys. Rev., vol. 92, no. 1, Oct. 1, 1953, pp. 45-51.

10. Bechtel, Robert T.: Component Testing of a 30-Centimeter-Diameter Electron Bombardment Thruster. Paper 70-1100, AIAA, Aug. 1970.

11. Dyke, W. P.; Charbonnier, F. M.; Strayer, R. W.; Floyd, R. L.; Barbour, J. P.; and Trolan, J. K.: Electrical Stability and Life of the Heated Field Emission Cathode. J. Appl. Phys., vol. 31, no. 5, May 1960, pp. 790-805.

12. Bettler, Philip C.; and Charbonnier, Francis M.: Activation Energy for the Surface Migration of Tungsten in the Presence of a High-Electric Field. Phys. Rev., vol. 119, no. 1, July 1, 1960, pp. 85-93.

13. Dyke, W. P.; Trolan, J. K.; Dolan, W. W.; and Barnes, George: The Field Emitter: Fabrication, Electron Microscopy, and Electric Field Calculations. J. Appl. Phys., vol. 24, no. 5, May 1953, pp. 570-576.

14. Drechsler, Michael M.: Kristallstufen von 1 bis 1000 Å. Zeit. f. Elektrochem., vol. 61, no. 1, 1957, pp. 48-55.

15. Gjostein, N. A.: Surface Self-Diffusion in FCC and BCC Metals: A Comparison of Theory and Experiment. Surfaces and Interfaces I: Chemical and Physical Characteristics. J. J. Burke, N. L. Reed and Volker Weiss, eds., Syracuse Univ. Press, 1967, pp. 271-304.

16. Dyke, W. P.; and Dolan, W. W.: Field Emission. Advances in Electronics and Electron Physics. Vol. 8. L. Morton, ed., Academic Press, 1956, pp. 89-185.

17. Drechsler, M.; Pankow, G.; and Vaneslow, R.: Evidence of Dislocations in the Decomposition of Tungsten, Tantalum, and Nickel Single Crystals. Z. Physik. Chem., vol. 4, 1955, pp. 249-263.

18. Louat, N.; and Wain, H. L.: Brittle Fracture and the Yield-Point Phenomenon. Fracture. B. L. Averbach, D. K. Felback, G. T. John and D. A. Thomas, eds., Technology Press of MIT and John Wiley & Sons, Inc., 1959, pp. 161-180.

TABLE I. - COMPARISON OF MEASURED

AND CALCULATED EVAPORATION

FIELD STRENGTHS

| Element | Calculated | | Experimental |
| | n = 1 | n = 2 | |
	Evaporation field strength, V/m ($V/Å \times 10^{-10}$)		
Boron	6.48×10^{10}	7.65×10^{10}	---------
Tungsten	6.90	5.50	5.70×10^{10}
Iridium	6.05	5.03	5.00
Molybdenum	4.77	4.52	4.50
Platinum	5.04	4.42	4.75
Rhenium	6.64	4.34	4.80
Rhodium	4.44	4.07	---------
Gold	4.02	4.85	3.50
Beryllium	5.40	3.84	3.40
Ruthenium	4.35	3.66	4.50
Palladium	3.63	4.08	---------
Cobalt	4.18	3.49	3.70
Niobium	5.26	3.48	4.00
Nickel	3.36	3.30	3.60
Iron	4.06	3.18	3.60
Silicon	4.43	3.17	3.00
Copper	3.08	4.30	3.00
Zinc	2.87	3.35	---------
Zirconium	4.52	2.84	3.50
Germanium	3.34	2.73	---------
Chromium	2.68	2.64	---------
Vanadium	3.84	2.50	---------
Titanium	3.53	2.33	2.50
Silver	2.31	4.42	---------
Tin	2.24	4.70	---------
Aluminum	1.61	3.28	---------

TABLE II. - EXPERIMENTAL CONDITIONS FOR

BULK SLIP IN APEX REGION

Point	Temperature, K	Field, V/m ($V/Å \times 10^{-10}$)	Surface polarity	Reference
1	1000	2×10^{10}	+	3
2	1100	1.7	+	10
3	1400	.8	+	10
4	1500	.65	-	10
5	1800	.52	-	10
6	2400	.375	+	10

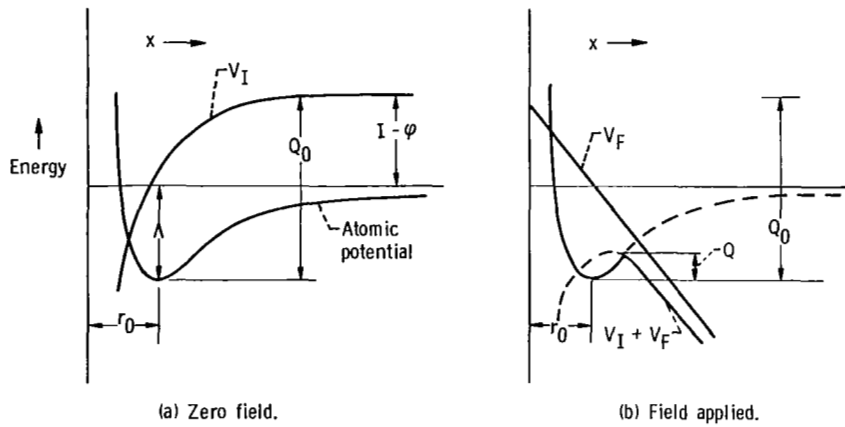(a) Zero field.   (b) Field applied.

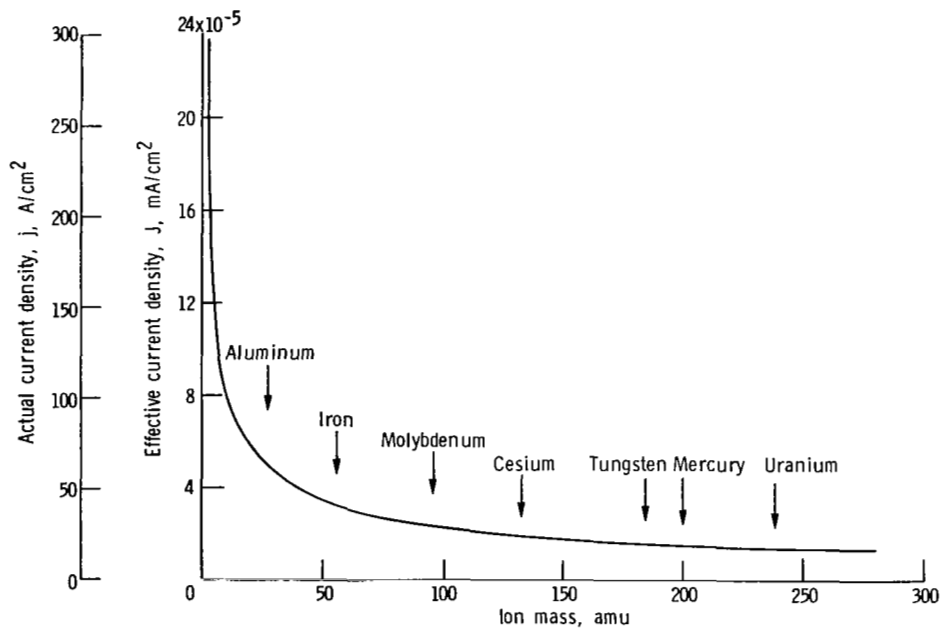Figure 1. – Potential diagram illustrating field-evaporation process.

Figure 2. – Space-charge-limited current density as function of ion mass.
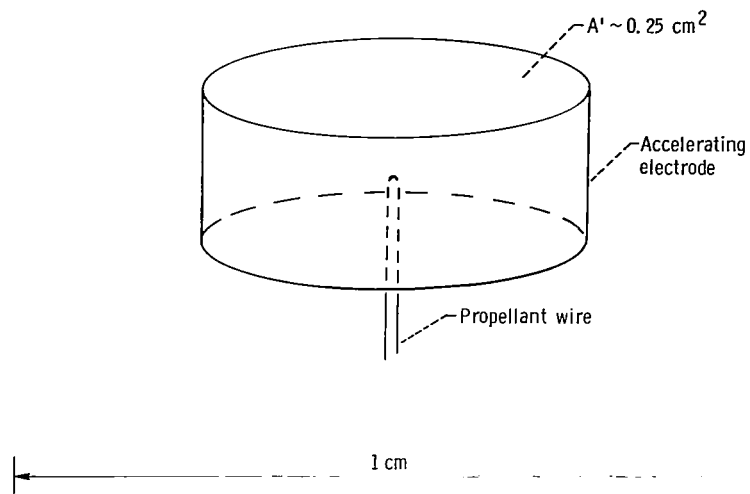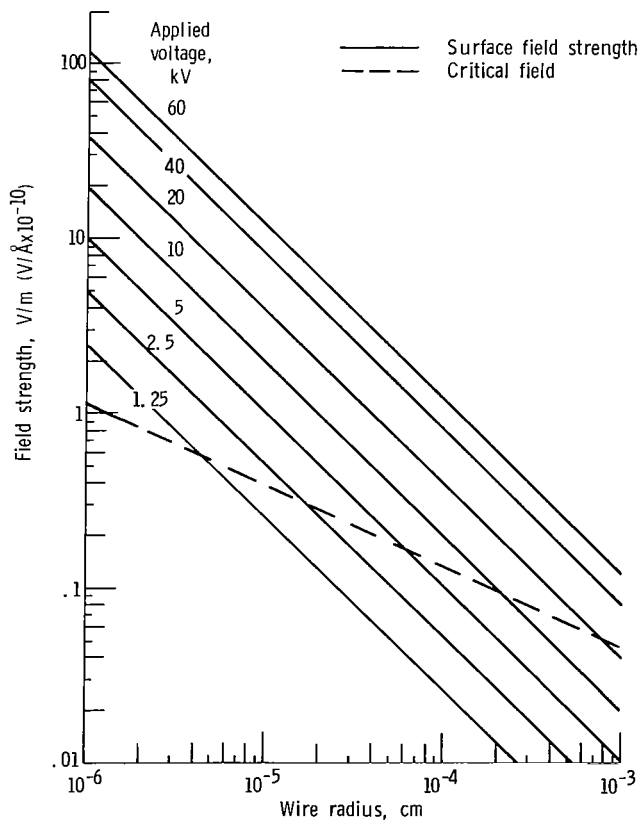
Figure 3. - Diagram of electrode geometry.

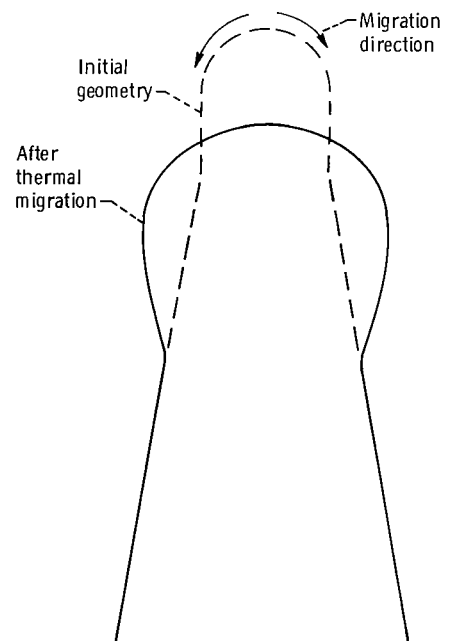Figure 4. - Field strength as function of wire radius.

Figure 5. - Schematic diagram of geometry change resulting from thermally induced surface migration (zero field).
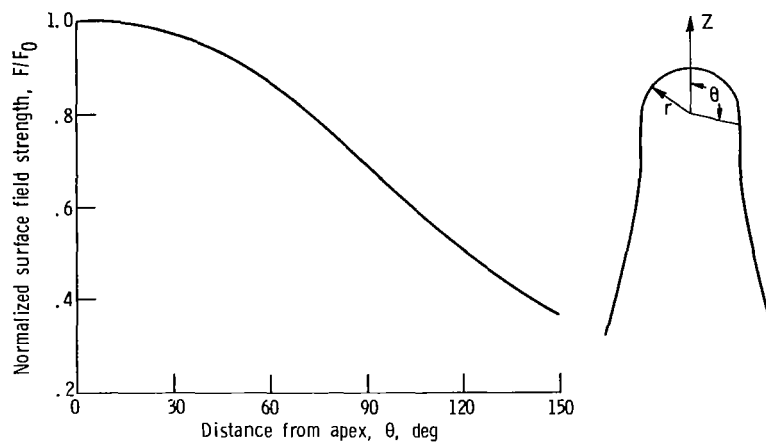
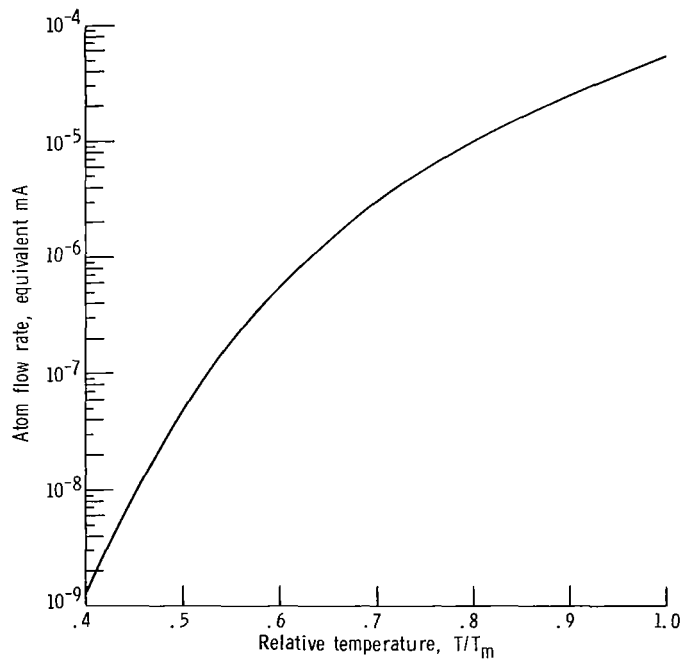Figure 6. – Variation of surface field strength with distance from apex. When $\theta = 0$, $F = F_0$.

Figure 7. – Calculated variation of surface-migration-limited current from one emitter as function of temperature (from eq. (6)). Wire radius, 10^{-4} centimeter; surface field, 7×10^7 volts per centimeter; critical field, 1.2×10^7 volts per centimeter; activation energy, 2.44 eV (ref. 5).
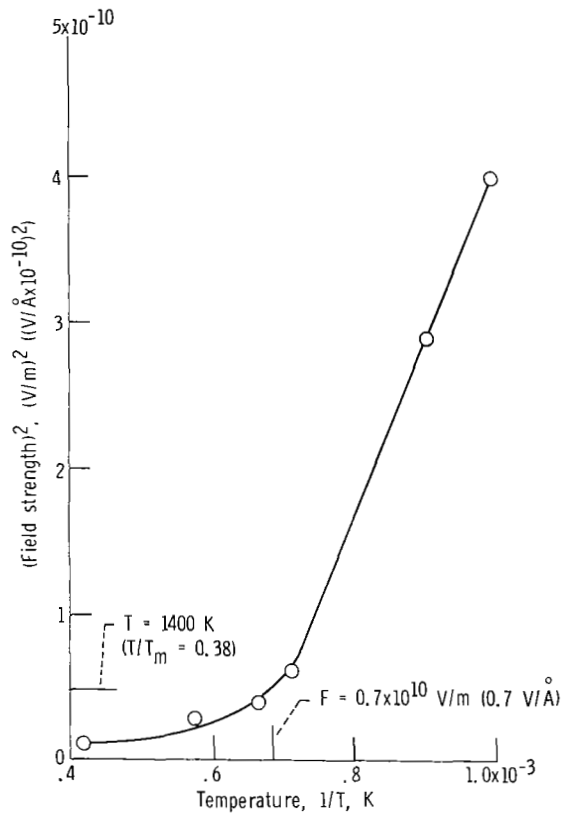
Figure 8. - Square of field strength in apex region as function of temperature. Note that bulk yield stress is proportional to square of surface field strength.
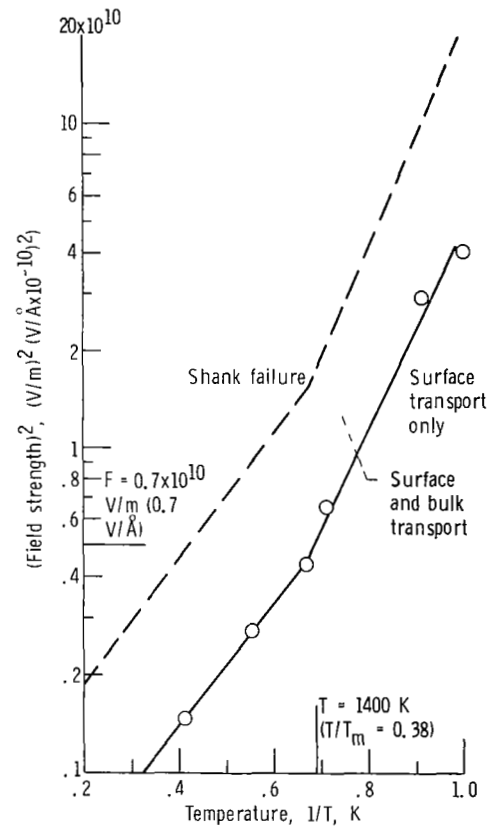

Figure 9. - Field-temperature relation required for bulk slip in apex region (solid curve) and in shank region (dashed curve).